

Multi-species modeling in the particle-based ellipsoidal statistical Bhatnagar-Gross-Krook method including internal degrees of freedom

F. Hild^{1, a)} and M. Pfeiffer^{1, b)}*Institute of Space Systems, University of Stuttgart, Pfaffenwaldring 29, 70569 Stuttgart, Germany*

(Dated: 11 August 2023)

The implementation of the ellipsoidal statistical Bhatnagar-Gross-Krook (ESBGK) method in the open-source particle code PICLas is extended for multi-species modeling of polyatomic molecules, including internal energies with multiple vibrational degrees of freedom. For this, the models of Mathiaud, Mieussens, and Pfeiffer¹, Pfeiffer² and Brull^{3,4} are combined. In order to determine the transport coefficients of the gas mixture, Wilke's mixing rules and collision integrals are compared. The implementation is verified with simulation test cases of a supersonic Couette flow as well as a hypersonic flow around a 70° blunted cone. The solutions of the ESBGK method are compared to the Direct Simulation Monte Carlo (DSMC) method to assess the accuracy, where overall good agreement is achieved. In general, collision integrals should be preferred for the determination of the transport coefficients, since the results using Wilke's mixing rules show larger deviations in particular for large mass ratios. Considering the computational efficiency of the methods, a considerable reduction in computational time is possible with the ESBGK model.

Keywords: DSMC, Ellipsoidal statistical BGK, Multi-species, Mixture, Internal degrees of freedom

I. INTRODUCTION

Numerical simulations of fluid dynamics in space applications, micro and nano flows, and vacuum technology present significant challenges for applied numerical methods. These applications involve large density gradients, ranging from the continuum to the free molecular flow regime, and require versatile numerical approaches due to their multi-scale and non-equilibrium nature. Although a highly accurate solution of these flows can be achieved by using the well-established Direct Simulation Monte Carlo (DSMC)⁵ method, the latter requires excessive computational effort in the transitional and continuum regimes. Thus, coupling DSMC with a computationally efficient method is desirable.

For continuum flows, computational fluid dynamics (CFD) are typically used. However, many problems arise in the coupling with the DSMC method due to the very different underlying approaches of both methods. Especially the statistical noise of the DSMC method is problematic at the boundaries between DSMC and CFD⁶⁻⁹.

Particle-based continuum methods have emerged as promising alternatives, bridging the transitional regime. Recent developments include but are not limited to the Fokker-Planck approach^{10,11} and the Bhatnagar-Gross-Krook (BGK)^{12,13} model, which is the focus of this paper. The latter approximates the collision integral of the Boltzmann equation by a relaxation process. With this, the mean free path and the collision frequency do not need to be resolved, making the choice of time step and particle weighting factor for particle simulations less restrictive. Thus, less computational costs are expected

compared to DSMC simulations, in particular for low- Kn regimes.

The particle-based ellipsoidal statistical BGK (ESBGK)¹⁴ and the Shakhov BGK¹⁵ methods were investigated in particular, both producing the correct Prandtl number of the gas. It was shown that the ESBGK model is more robust and more efficient in the particle context¹⁶, which is why this approach is followed here. An overview of different BGK models for gas mixtures is available from Pirner¹⁷.

The focus of this paper is the extension of the particle-based ESBGK model to gas mixtures including non-equilibrium states of internal degrees of freedom of di- and polyatomic molecules, including quantized vibrational states. The work is based on the models of Mathiaud, Mieussens, and Pfeiffer¹, Pfeiffer² and Brull^{3,4}.

II. THEORY

The BGK operator is an approximation of the Boltzmann collision integral as relaxation process of the particle distribution function $f_s(\mathbf{x}, \mathbf{v}, t)$ of a species s at position \mathbf{x} and with velocity \mathbf{v} towards a target distribution f_s^{t12}

$$\partial_t f_s + \mathbf{v} \partial_{\mathbf{x}} f_s = \nu (f_s^t - f_s), \quad (1)$$

using the relaxation frequency ν . In a mixed model of atoms and molecules, the target distribution function differs between the two because the internal degrees of freedom (DOF) for the molecules must be taken into account. While the atoms only carry translational DOFs, the molecules carry vibrational and rotational DOFs additionally. Therefore, the target distribution function of atoms only consists of a translational part

$$f_{s, \text{Atom}}^t = f_s^{t, \text{tr}}(\mathbf{v}), \quad (2)$$

^{a)}Electronic mail: hildf@irs.uni-stuttgart.de

^{b)}Electronic mail: mpfeiffer@irs.uni-stuttgart.de

depending on the particle velocity \mathbf{v} , whereas the distribution function for molecules can be separated into the translational, the rotational and the vibrational part as demonstrated in Mathiaud, Mieussens, and Pfeiffer¹, Dauvois, Mathiaud, and Mieussens¹⁸

$$f_s^t, \text{Molecule} = f_s^{t, \text{tr}}(\mathbf{v}) f_s^{t, \text{rot}}(E_{\text{rot}}) f_s^{t, \text{vib}}(i_{\text{vib}}), \quad (3)$$

depending also on the rotational energy E_{rot} and the vibrational quantum number i_{vib} .

A. Macroscopic Flow Values

The macroscopic flow values particle density n , flow velocity u and temperature T_{tr} of each species s are defined as the moments of the particle distribution function:

$$n_s = \int_{\mathbb{R}^3} f_s^{\text{tr}} d\mathbf{v}, \quad n_s \mathbf{u}_s = \int_{\mathbb{R}^3} \mathbf{v} f_s^{\text{tr}} d\mathbf{v}, \quad (4)$$

$$\mathcal{E}_s = \frac{3}{2} k_B T_{\text{tr},s} = \frac{m_s}{2n_s} \int_{\mathbb{R}^3} \mathbf{c}_s^2 f_s^{\text{tr}} d\mathbf{v}, \quad (5)$$

$$E_s = \frac{1}{2} m_s n_s \mathbf{u}_s^2 + n_s \mathcal{E}_s, \quad (6)$$

with the thermal particle velocity $\mathbf{c} = \mathbf{v} - \mathbf{u}$ from the particle velocity \mathbf{v} . Furthermore, the macroscopic mean values of the flow are given by:

$$\rho = \sum_{s=1}^M m_s n_s, \quad \rho \mathbf{u} = \sum_{s=1}^M m_s n_s \mathbf{u}_s, \quad (7)$$

$$n \mathcal{E} + \frac{\rho}{2} \mathbf{u}^2 = E = \sum_{s=1}^M E_s, \quad \mathcal{E} = \frac{3}{2} k_B T_{\text{tr}}. \quad (8)$$

For molecular species, it is also necessary to define the mean rotational energy $\langle E \rangle_{\text{rot}}$ and the mean vibrational energy $\langle E \rangle_{\text{vib}}$, which are directly linked to the rotational temperature T_{rot} and the vibrational temperature T_{vib} :

$$\langle E \rangle_{\text{rot},s} = \frac{\xi_{\text{rot},s}}{2} k_B T_{\text{rot},s} = \frac{1}{n_s} \int E_{\text{rot}} f_s^{\text{rot}} dE_{\text{rot}}, \quad (9)$$

$$\langle E \rangle_{\text{vib},s} = \sum_{j=1}^{\gamma} \frac{\xi_{\text{vib},j,s}}{2} k_B T_{\text{vib},s} \quad (10)$$

$$= \frac{1}{n_s} \sum_{j=1}^{\gamma} \sum_{i_{\text{vib},j}} k_B \Theta_{\text{vib},j,s} f_s^{\text{vib}}. \quad (11)$$

ξ are the degrees of freedom of rotation and vibration. In the diatomic case, $\xi_{\text{rot}} = 2$ applies, while in the polyatomic case, $\xi_{\text{rot}} = 2$ applies for linear molecules and $\xi_{\text{rot}} = 3$ for non-linear molecules^{19,20}. For the vibration, the simple harmonic oscillator (SHO) model is assumed with the characteristic vibrational temperature Θ_{vib} . Due to the quantization, the degrees of freedom are not fixed but temperature-dependent. In the polyatomic

case, γ is the number of vibration modes as a function of the total number of atoms a in the molecule¹⁹:

$$\gamma = \begin{cases} 3a - 5, & \text{linear molecule,} \\ 3a - 6, & \text{non-linear molecule.} \end{cases} \quad (12)$$

In the case of a diatomic molecule, $\gamma = 1$ follows. With the assumption of the SHO, an expression for the mean energy and vibration degrees of freedom as a function of temperature $T_{\text{vib},s}$ can be found:

$$\langle E \rangle_{\text{vib},s} = \sum_{j=1}^{\gamma} \frac{k_B \Theta_{\text{vib},j,s}}{\exp(\Theta_{\text{vib},j,s}/T_{\text{vib},s}) - 1}, \quad (13)$$

$$\xi_{\text{vib},s} = \sum_{j=1}^{\gamma} \xi_{\text{vib},j,s} = \sum_{j=1}^{\gamma} \frac{2\Theta_{\text{vib},j,s}/T_{\text{vib},s}}{\exp(\Theta_{\text{vib},j,s}/T_{\text{vib},s}) - 1}. \quad (14)$$

B. ESBGK mixture model

The model proposed here combines the model of Mathiaud, Mieussens, and Pfeiffer¹, Pfeiffer² and the model of Brull^{3,4} into a mixture model that allows for non-equilibrium effects in the internal degrees of freedom. Different than the standard BGK model using a Maxwellian target distribution function, the ellipsoidal statistical BGK (ESBGK) model produces the correct Prandtl number by using an anisotropic Gaussian distribution¹⁴

$$f_s^{\text{ES, tr}} = \frac{\rho_s}{\sqrt{\det 2\pi \mathcal{A}_s}} \exp\left[-\frac{1}{2} \mathbf{c}^T \mathcal{A}_s^{-1} \mathbf{c}\right] \quad (15)$$

with the mass density of the considered species ρ_s and the average flow velocity \mathbf{u} . The anisotropic matrix \mathcal{A}_s reads:

$$\mathcal{A}_s = \frac{k_B T_{\text{tr,rel}}}{m_s} \mathcal{I} - \frac{1 - \alpha Pr}{\alpha Pr} \frac{k_B}{m_s} \left(\frac{T_{\text{tr,rel}}}{T_{\text{tr}}} \mathcal{P} - T_{\text{tr,rel}} \mathcal{I} \right) \quad (16)$$

and consists of the identity matrix \mathcal{I} and the pressure tensor \mathcal{P}

$$\mathcal{P} = \frac{1}{\rho} \sum_{s=1}^M m_s \int (\mathbf{v} - \mathbf{u})(\mathbf{v} - \mathbf{u})^T f_s d\mathbf{v}, \quad (17)$$

which are both symmetric³. The parameter α is a variable of the model depending on mass fraction, density fraction and internal degrees of freedom⁴:

$$\alpha = m \frac{\sum_{s=1}^M \frac{n_s}{m_s} (5 + \xi_{\text{int},s})}{\sum_{s=1}^M n_s (5 + \xi_{\text{int},s})}, \quad (18)$$

$$m = \sum_{s=1}^M \frac{n_s}{n} m_s, \quad n = \sum_{s=1}^M n_s. \quad (19)$$

The internal degrees of freedom are calculated as the sum of the vibrational and rotational degrees of freedom, respectively:

$$\xi_{\text{int},s} = \xi_{\text{vib},s} + \xi_{\text{rot},s}. \quad (20)$$

The model used and presented in this paper uses one relaxation term per species s . It fulfills the indifferentiability principle so that the model reduces to a single species model for identical species. Additionally, the Maxwellian distribution is produced in the equilibrium state. The relaxation frequency ν of the model is defined by

$$\nu = \frac{nk_B T_{\text{tr}}}{\mu} \alpha Pr \quad (21)$$

with the viscosity of the mixture μ and the translational temperature T_{tr} . Pr is the targeted Prandtl number of the gas mixture, which is calculated using Wilke's mixing rules²¹ or collision integrals²² (see Section II C).

For molecular species, the rotational and vibrational components of the distribution function must also be defined, which are taken directly from Mathiaud, Mieussens, and Pfeiffer¹:

$$f_s^{\text{ES,rot}} = \frac{E_{\text{rot}}^{(\xi_{\text{rot},s}-2)/2}}{\Gamma(\xi_{\text{rot},s}/2) (k_B T_{\text{rot,rel},s})^{\xi_{\text{rot},s}/2}} \cdot \exp\left[-\frac{E_{\text{rot}}}{k_B T_{\text{rot,rel},s}}\right], \quad (22)$$

$$f_s^{\text{ES,vib}} = \prod_{j=1}^{\gamma} \left(1 - \exp\left[-\frac{\Theta_{\text{vib},j,s}}{T_{\text{vib,rel},s}}\right]\right) \cdot \exp\left[-i_j \frac{\Theta_{\text{vib},j,s}}{T_{\text{vib,rel},s}}\right]. \quad (23)$$

The temperatures $T_{\text{tr,rel}}$, $T_{\text{rot,rel},s}$ and $T_{\text{vib,rel},s}$ introduced here are chosen so that the relaxation corresponds to the Landau-Teller relaxation:

$$\frac{d\langle E \rangle_{r,s}(T_{r,s})}{dt} = \frac{1}{Z_{r,s} \tau_{s,C}} \left(\langle E \rangle_{r,s}(T_{\text{tr}}) - \langle E \rangle_{r,s}(T_{r,s}) \right), \quad (24)$$

$r = \text{rot, vib.}$

Here $Z_{r,s}$ is the collision number of the internal degrees of freedom r per species s and $\tau_{s,C} = 1/\nu_{s,C}$ is the collision time of the gas per species. The latter is different from $\tau = 1/\nu$, the relaxation time of the BGK equation (1), whereas a detailed discussion can be found in Mathiaud, Mieussens, and Pfeiffer¹. The collision frequency for the variable hard sphere model (VHS) of each species s in a mixture of M species is calculated by²³:

$$\nu_{s,C} = \sum_{k=1}^M 2d_{s,k}^2 n_k \sqrt{\frac{2\pi k_B T_{s,k}}{(m_s + m_k)}} m_s m_k \left(\frac{T_{s,k}}{T_{\text{tr}}}\right)^{\omega_{s,k}} \quad (25)$$

with

$$d_{s,k} = 0.5 (d_{\text{ref},s} + d_{\text{ref},k}), \quad (26)$$

$$T_{s,k} = 0.5 (T_{\text{ref},s} + T_{\text{ref},k}), \quad (27)$$

$$\omega_{s,k} = 0.5 (\omega_{\text{VHS},s} + \omega_{\text{VHS},k}). \quad (28)$$

If direct VHS data are available for each collision combination, these can also be used accordingly here²⁴⁻²⁶.

With these definitions, $T_{\text{tr,rel}}$, $T_{\text{rot,rel},s}$ and $T_{\text{vib,rel},s}$ can now be defined with $r = \text{rot, vib}$:

$$\langle E \rangle_{r,s}(T_{r,\text{rel},s}) = \langle E \rangle_{r,s}(T_{r,s}) + \frac{\tau}{Z_{r,s} \tau_{s,C}} \left(\langle E \rangle_{r,s}(T_{\text{tr}}) - \langle E \rangle_{r,s}(T_{r,s}) \right), \quad (29)$$

$$\langle E \rangle_{\text{tr}}(T_{\text{tr,rel}}) = \langle E \rangle_{\text{tr}}(T_{\text{tr}}) - \sum_r \sum_s^{M_{\text{molec}}} \frac{\tau}{Z_{r,s} \tau_{s,C}} \left(\langle E \rangle_{r,s}(T_{\text{tr}}) - \langle E \rangle_{r,s}(T_{r,s}) \right). \quad (30)$$

C. Gas mixture properties

The ESBGK model requires the calculation of the correct Prandtl number

$$Pr = c_p \frac{\mu}{K} \quad (31)$$

of the gas mixture to assess the relaxation frequency from Equation (21). Here, μ is the viscosity, K is the thermal conductivity and c_p is the specific heat of the considered mixture. The latter is calculated as:

$$c_p = \sum_{s=1}^M \frac{5 + \xi_{\text{int},s}}{2} k_B \frac{n_s}{\sum_{k=1}^M n_k m_k}. \quad (32)$$

For the calculation of the mixture viscosity and thermal conductivity, any source can be used in the presented model. Basically, the same problems also arise with multi-species CFD codes and therefore the same solutions can also be applied. Typically, the transport properties are calculated on the basis of Wilke's mixture rules²¹ or the first approximation of the transport properties using collision integrals²², whereby various libraries are also available that can be used directly²⁷⁻²⁹. However, in order to achieve the same transport coefficients as far as possible when coupling with DSMC, the procedure for the Variable Hard Sphere (VHS) potential model is presented in this paper.

1. Wilke's mixing rules

Wilke's mixing rules²¹ are used for the calculation of the transport coefficients of the mixture. The well-known exponential ansatz is used for the viscosity of each species μ_s , which can be calculated with:

$$\mu_s = \mu_{\text{ref},s} \left(\frac{T_{\text{tr}}}{T_{\text{ref},s}} \right)^{\omega_{\text{VHS},s}}. \quad (33)$$

Here, $\mu_{\text{ref},s}$ is the reference dynamic viscosity at a reference temperature $T_{\text{ref},s}$ for each species s , and $\omega_{\text{VHS},s}$ is a species-specific parameter of the Variable Hard Sphere (VHS) model^{5,24-26}. Using the VHS reference diameter

$d_{\text{ref},s}$, the reference dynamic viscosity for a VHS gas is defined as³⁰:

$$\mu_{\text{ref},s} = \frac{30\sqrt{mk_{\text{B}}T_{\text{ref},s}}}{\sqrt{\pi}4(5 - 2\omega_{\text{VHS},s})(7 - 2\omega_{\text{VHS},s})d_{\text{ref},s}^2}. \quad (34)$$

The mixture viscosity of M species is then calculated by²¹:

$$\mu = \sum_{s=1}^M n_s \frac{\mu_s}{\Phi_s}, \quad \Phi_s = \sum_{k=1}^M n_k \frac{\left(1 + \sqrt{\frac{\mu_s}{\mu_k}} \left(\frac{m_k}{m_s}\right)^{1/4}\right)^2}{\sqrt{8\left(1 + \frac{m_s}{m_k}\right)}}. \quad (35)$$

The thermal conductivity of each species K_s can be calculated using the Eucken's relation³¹ and the correction by Hirschfelder³² with the viscosity:

$$K_s = (f_{\text{tr}}c_{v,\text{tr},s} + f_{\text{int}}c_{v,\text{int},s})\mu_s. \quad (36)$$

Here, $c_{v,s} = \xi_s k_{\text{B}}/2m_s$ is the specific heat capacity at constant volume for species s , with the corresponding degrees of freedom for translation $\xi_{\text{tr}} = 3$ for each species and the internal degrees of freedom $\xi_{\text{int},s}$ from Equation (20). In general, $c_v = c_p - k_{\text{B}}/m$ applies. The prefactors used in Equation (36) are defined as $f_{\text{tr}} = 5/2$ and $f_{\text{int}} = 1.328$. With that, the thermal conductivity of the mixture K is calculated:

$$K = \sum_{s=1}^M n_s \frac{K_s}{\Phi_s}. \quad (37)$$

2. First approximation of transport properties

Another calculation possibility is the first approximation to the viscosity of species s depending on the collision integral $\Omega_s^{(2)}(2)$, which is given by²²

$$\mu_s = \frac{5k_{\text{B}}T_{\text{tr},s}}{8\Omega_s^{(2)}(2)}. \quad (38)$$

The mixture viscosity is determined by

$$\mu = \sum_{s=1}^M b_s, \quad (39)$$

where b_s is the contribution of each species to the total mixture viscosity and is determined by solving the system

$$\chi_s = b_s \left(\frac{\chi_s}{\mu_s} + \sum_{k \neq s} \frac{3\chi_s}{(\rho'_k + \rho'_s)D_{sk}} \left(\frac{2}{3} + \frac{m_k}{m_s} A_{sk} \right) \right) - \chi_s \sum_{k \neq s} \frac{3b_k}{(\rho'_k + \rho'_s)D_{sk}} \left(\frac{2}{3} - A_{sk} \right) \quad (40)$$

with the mole fraction χ , the density ρ'_k of species k when pure at pressure and temperature of the actual gas mixture, the parameter A_{sk} , defined by

$$A_{sk} = \frac{\Omega_{sk}^{(2)}(2)}{5\Omega_{sk}^{(1)}(1)}, \quad (41)$$

and the binary diffusion coefficient with the reduced mass m_{sk}^* :

$$D_{sk} = \frac{3k_{\text{B}}T_{\text{tr}}}{16nm_{sk}^*\Omega_{sk}^{(1)}(1)}. \quad (42)$$

The mixture thermal conductivity K is calculated by

$$K = \sum_{s=1}^M a_s + \sum_{s=1}^{M_{\text{molec}}} K_{\text{rot},s} + \sum_{s=1}^{M_{\text{molec}}} K_{\text{vib},s}, \quad (43)$$

with a_s being the translational species contribution to the total mixture thermal conductivity and $K_{\text{rot},s}$ as well as $K_{\text{vib},s}$ being the rotational and vibrational contributions of the species s ²³. The factors a_s are determined by solving the system

$$\begin{aligned} \chi_s = a_s & \left[\frac{\chi_s}{K_s} + \sum_{k \neq s} \frac{\chi_k}{5k_{\text{B}}nD_{sk}} \cdot \left(6 \left(\frac{m_s}{m_k + m_s} \right)^2 \right. \right. \\ & \left. \left. + (5 - 4B_{sk}) \left(\frac{m_k}{m_k + m_s} \right)^2 + 8 \frac{m_k m_s}{(m_s + m_k)^2} A_{sk} \right) \right] \\ & - \chi_s \sum_{k \neq s} a_k \frac{m_k m_s}{(m_s + m_k)^2} (5k_{\text{B}}nD_{sk})^{-1} \\ & \cdot (11 - 4B_{sk} - 8A_{sk}). \end{aligned} \quad (44)$$

Here, K_s is the first approximation of the thermal conductivity of species s :

$$K_s = \frac{25c_{v,\text{tr},s}k_{\text{B}}T_{\text{tr},s}}{16\Omega_s^{(2)}(2)}, \quad c_{v,\text{tr},s} = \frac{3k_{\text{B}}}{2m_s}, \quad (45)$$

and the parameter B_{sk} is defined by

$$B_{sk} = \frac{5\Omega_{sk}^{(1)}(2) - \Omega_{sk}^{(1)}(3)}{5\Omega_{sk}^{(1)}(1)}. \quad (46)$$

The collision integrals for the VHS model are given by³³

$$\begin{aligned} \Omega_{sk}^{\text{VHS},(1)}(1) &= \frac{\pi}{2} d_{\text{ref}}^2 \sqrt{\frac{k_{\text{B}}T_{\text{tr}}}{2\pi m_{sk}^*}} \left(\frac{T_{\text{ref}}}{T_{\text{tr}}} \right)^{\omega-1/2} \frac{\Gamma(7/2 - \omega)}{\Gamma(5/2 - \omega)} \\ \Omega_{sk}^{\text{VHS},(2)}(2) &= \frac{\pi}{3} d_{\text{ref}}^2 \sqrt{\frac{k_{\text{B}}T_{\text{tr}}}{2\pi m_{sk}^*}} \left(\frac{T_{\text{ref}}}{T_{\text{tr}}} \right)^{\omega-1/2} \frac{\Gamma(9/2 - \omega)}{\Gamma(5/2 - \omega)} \\ B_{sk}^{\text{VHS}} &= \frac{5\Gamma(9/2 - \omega) - \Gamma(11/2 - \omega)}{5\Gamma(7/2 - \omega)} \end{aligned} \quad (47)$$

with the VHS parameters d_{ref} , T_{ref} and ω . Generally, for $s = k$, the translational temperature of the species $T_{\text{tr},s}$

is used, while for $s \neq k$, the translational temperature in the cell T_{tr} is used as an approximation in order to reduce noise.

The rotational and vibrational contributions $K_{r,s}$ with $r = \text{rot, vib}$ to the thermal conductivity of a species s are calculated as²³:

$$K_{r,s} = \frac{n_s m_s c_{v,r,s}}{\sum_{k=1}^M \chi_k D_{sk}^{-1}}, \quad c_{v,r,s} = \frac{\xi_{r,s} k_B}{2m_s}. \quad (48)$$

III. IMPLEMENTATION

The proposed ESBGK method gas mixtures with internal degrees of freedom is implemented in the open-source particle code PICLas³⁴. A stochastic particle approach is chosen for the implementation^{2,16,35,36}, although the model can of course also be used in discrete velocity (DVM) codes. Especially to save simulation time in DVM multi-species simulations, the model should be extended to a reduced model in the future^{1,18,37}.

A. Relaxation and sampling

Regarding movement and boundary conditions, particles are treated in the same manner as in the DSMC method. But instead of performing binary collisions between the particles, all particles in a cell relax with a probability P in each time step Δt :

$$P = 1 - \exp[-\nu \Delta t], \quad (49)$$

which corresponds to Eq. (1) in a stochastic interpretation as described in Pfeiffer¹⁶. The first order method from Pfeiffer¹⁶ is used here. In the future, however, this model will be extended to the second-order particle method from Pfeiffer, Garmirian, and Gorji³⁸. The relaxation frequency ν , which is the same as in Equation (1), is evaluated in each time step for each cell according to Equation (21) using the transport coefficients of the mixture calculated in the code.

The particles that are chosen to relax are then sampled from the target distribution (see Equation (15)). Here, an approximation of the transformation matrix \mathcal{S} ³⁹ with $\mathcal{A} = \mathcal{S}\mathcal{S}$ is used to transform a random vector chosen from a Maxwellian to a velocity vector chosen from the ESBGK distribution:

$$v_p^* = u + \mathcal{S} \sqrt{R_p \frac{k_B T_{\text{tr,rel}}}{m_s}}. \quad (50)$$

For a detailed description of the sampling process, the reader is referred to Ref.¹⁶, in which also alternative methods for sampling are described.

At this point, a special solution for the stochastic particle approach must be chosen. Even though the presented model is both momentum and energy conserving, additional effort must be made for both in a stochastic

approach. The basic problem is that the new states of the particles (velocities, internal energies) are chosen randomly from the distribution functions. Thus, in this random step, conservation of energy and momentum is not automatically given and one would need a large number of particles for stable simulations. To construct energy conservation for the stochastic particle method, the energy difference between the old and new sampled energy must be distributed over the particles in such a way that energy conservation is given. The idea is to distribute this energy difference evenly according to the respective degrees of freedom to the translational energy of all particles in the cell and the internal degrees of freedom of the particles relaxing in the degrees of freedom within the cell, as this has led to the best results in previous work². An artificial equilibrium temperature T_{equi} is introduced for this purpose. Starting from this point, molecules are chosen to relax in the rotation and vibration towards the equilibrium temperature T_{equi} with the probability

$$P_{r,s} = P \beta_{r,s} \frac{\tau}{Z_{r,s} \tau_{s,C}}, \quad r = \text{rot, vib}, \quad (51)$$

so that Eq. (1), Eq. (22) and Eq. (23) are fulfilled. To save calculation time, instead of using the probability P to relax the particles to $T_{\text{vib,rel},s}$ and $T_{\text{rot,rel},s}$ corresponding to Eq. (22) and Eq. (23), only the fraction $\frac{\tau}{Z_{r,s} \tau_{s,C}}$ relaxes directly to T_{tr} according to equation Eq. (29), which leads to the same result but with significantly fewer relaxing particles. Additionally, a correction parameter $\beta_{r,s}$ for the rotation and vibration, respectively, is defined per species in order to follow the idea of equal distribution of energies for the conservation of energy as described:

$$\begin{aligned} & \frac{\tau}{Z_{r,s} \tau_{s,C}} \left(\langle E \rangle_{r,s}(T_{\text{tr}}) - \langle E \rangle_{r,s}(T_{r,s}) \right) \\ &= \beta_{r,s} \frac{\tau}{Z_{r,s} \tau_{s,C}} \left(\langle E \rangle_{r,s}(T_{\text{equi}}) - \langle E \rangle_{r,s}(T_{r,s}) \right) \\ &\Rightarrow \beta_{r,s} = \frac{T_{r,s} - T_{\text{tr}}}{T_{r,s} - T_{\text{equi}}}. \end{aligned} \quad (52)$$

Since T_{equi} directly depends on $\beta_{\text{rot},s}$ and $\beta_{\text{vib},s}$ of each species, the solution of this equation system is obtained numerically. For this purpose, the following system must be solved:

$$\begin{aligned} T_{\text{equi}}^{n+1} = & \left[3(N-1)T_{\text{tr}} + \sum_{s=1}^{M_{\text{molec}}} \xi_{\text{rot},s} N_s P_{\text{rot},s}(\beta_{\text{rot},s}^n) T_{\text{rot},s} \right. \\ & \left. + \sum_{s=1}^{M_{\text{molec}}} \xi_{\text{vib},s} N_s P_{\text{vib},s}(\beta_{\text{vib},s}^n) T_{\text{vib},s} \right] \\ & / \left[3(N-1) + \sum_{s=1}^{M_{\text{molec}}} \xi_{\text{rot},s} N_s P_{\text{rot},s}(\beta_{\text{rot},s}^n) \right. \\ & \left. + \sum_{s=1}^{M_{\text{molec}}} \xi_{\text{vib},s}(T_{\text{equi}}^n) N_s P_{\text{vib},s}(\beta_{\text{vib},s}^n) \right], \end{aligned} \quad (53)$$

$$\beta_{r,s}^{n+1} = \frac{T_{r,s} - T_{\text{tr}}}{T_{r,s} - T_{\text{equi}}^{n+1}}, \quad (54)$$

with the starting values

$$\beta_{r,s}^0 = 1, \quad (55)$$

$$\xi_{\text{vib},s}(T_{\text{equi}}^0) = \xi_{\text{vib},s}(T_{\text{vib},s}), \quad (56)$$

and iteration step n , until the accuracy ϵ is reached with the condition $T_{\text{equi}}^{n+1} - T_{\text{equi}}^n < \epsilon$. N is hereby defined as the total number of particles in the gas mixture, while N_s is the particle number per species.

The new rotational energy of a molecule p , which is chosen for a rotational relaxation according to the probability in Equation (51), is calculated by:

$$E_{\text{rot},p}^* = -\frac{\xi_{\text{rot},s}}{2} k_B T_{\text{equi}} \ln(R_p), \quad (57)$$

using a random number R_p . In the same manner, the new vibrational energy of a vibrational relaxing particle is calculated:

$$E_{\text{vib},p}^* = -\sum_{j=1}^{\gamma} \frac{\xi_{\text{vib},j,s}(T_{\text{equi}})}{2} k_B T_{\text{equi}} \ln(R_{p,j}). \quad (58)$$

The post-relaxation energies are hereby denoted with $*$. To fulfill the energy conservation, these energies need to be scaled additionally. Note: At this point the vibration is still continuous but already with the correct quantized degrees of freedom. The transition to quantized states happens with the conservation of energy.

B. Energy and momentum conservation

The energy and momentum conservation is based on Ref.² and extended to polyatomic molecules and mixtures of different gas species. In the implemented scheme, only relaxations in translation-vibration ($T - V$) and translation-rotation ($T - R$) are allowed directly. In the following, the process is described in greater detail. Here, the parameters after energy conservation are denoted with $'$.

For the energy conservation process, the vibrational energy is scaled first. The energy E_{T-V} is the sum of the total translational energy of the gas mixture and the vibrational energy of all relaxing particles in vibration, N_{vib} , before the relaxation process:

$$E_{T-V} = \sum_{p=1}^N \frac{m}{2} c_p^2 + \sum_{p=1}^{N_{\text{vib}}} \left(E_{\text{vib},p} - \sum_{j=1}^{\gamma} 0.5 k_B \Theta_{\text{vib},j,s} \right). \quad (59)$$

It should be distributed equally over all translational and vibrational DOFs after the relaxation process to fulfill the energy conservation. This is reached with a scaling

factor $\alpha_{\text{vib},s}$, that is calculated per species as:

$$\alpha_{\text{vib},s} = \frac{E_{T-V}}{\sum_{p=1}^{N_{\text{vib}}} E_{\text{vib},p}^*} \cdot \left(\frac{\xi_{\text{vib},s}(T_{\text{equi}}) N_{\text{vib},s}}{3(N-1) + \sum_{s=1}^{M_{\text{molec}}} \xi_{\text{vib},s}(T_{\text{equi}}) N_{\text{vib},s}} \right). \quad (60)$$

With this, the new vibrational energy of each particle p after the relaxation and energy conservation processes is

$$E'_{\text{vib},p} = \alpha_{\text{vib},s} E_{\text{vib},p}^* + \sum_{j=1}^{\gamma} 0.5 k_B \Theta_{\text{vib},j,s} \quad (61)$$

for the continuous handling of the vibrational energies and including the zero-point energy corresponding to the second sum. For quantized vibrational energy states, additional steps are to be performed. The energy per vibrational mode $\alpha_{\text{vib},s} E_{\text{vib},p,j}^*$ is reformulated to a quantum number $i_{p,j}$ with a random number $R_{p,j} \in [0, 1)$:

$$i_{p,j} = \text{INT} \left(\frac{\alpha_{\text{vib},s} E_{\text{vib},p,j}^*}{k_B \Theta_{\text{vib},j,s}} + R_{p,j} \right). \quad (62)$$

If the condition

$$E_{T-V} > i_{p,j} k_B \Theta_{\text{vib},j,s} \quad (63)$$

is fulfilled,

$$E'_{\text{vib},p,j} = (i_{p,j} + 0.5) k_B \Theta_{\text{vib},j,s} \quad (64)$$

is the new energy of this vibrational mode, including the zero-point energy. Otherwise, a new quantum number of this mode is calculated with a new random number $R_{p,j}$ as:

$$i_{p,j} = \text{INT} \left(-\ln(R_{p,j}) \frac{T_{\text{equi}}}{\Theta_{\text{vib},j,s}} \right) \quad (65)$$

until Equation (63) is fulfilled. $E'_{\text{vib},p,j}$ is then calculated with this new quantum number using Equation (64) subsequently. The energy E_{T-V} is subsequently updated with

$$E_{T-V} = E_{T-V} - i_{p,j} k_B \Theta_{\text{vib},j,s}, \quad (66)$$

before the algorithm is repeated for each vibrational mode j of each vibrational relaxing particle p . In the end, the new energy of the each particle p is:

$$E'_{\text{vib},p} = \sum_{j=1}^{\gamma} E'_{\text{vib},p,j}. \quad (67)$$

Afterwards, the remaining energy for translation and rotation is the sum of the remaining E_{T-V} and the rotational energy of all rotational relaxing particles before the relaxation process:

$$E_{T-R} = E_{T-V} + \sum_{p=1}^{N_{\text{rot}}} E_{\text{rot},p}. \quad (68)$$

Here, N_{rot} is the number of the rotational relaxing particles. E_{T-R} should be distributed equally over all translational and rotational DOFs similar to E_{T-V} . For this, a scaling factor $\alpha_{\text{rot},s}$ is calculated per species as:

$$\alpha_{\text{rot},s} = \frac{E_{T-R}}{\sum_{p=1}^{N_{\text{rot}}} E_{\text{rot},p}^*} \cdot \left(\frac{\xi_{\text{rot},s} N_{\text{rot},s}}{3(N-1) + \sum_{s=1}^{M_{\text{molec}}} \xi_{\text{rot},s} N_{\text{rot},s}} \right). \quad (69)$$

Using this, the new rotational energy of each particle p after the relaxation and energy conservation processes is calculated with:

$$E'_{\text{rot},p} = \alpha_{\text{rot},s} E_{\text{rot},p}^*. \quad (70)$$

Different than for the internal DOFs, and as described earlier, all particles in the gas mixture are scaled in the translation, whether they relax or not. The scaling factor α_{tr} is derived to be

$$\alpha_{\text{tr}} = \left[\frac{E_{T-R}}{\sum_{p=1}^N \frac{m}{2} (v_p^* - u^*)^2} \cdot \left(\frac{3(N-1)}{3(N+1) + \sum_{s=1}^{M_{\text{molec}}} \xi_{\text{rot},s} N_{\text{rot},s}} \right) \right]^{1/2}. \quad (71)$$

Finally, the new particle velocities are calculated using

$$v'_p = u + \alpha_{\text{tr}} (v_p^* - u^*), \quad (72)$$

with the average flow velocities

$$u = \sum_{p=1}^N v_p / N, \quad u^* = \sum_{p=1}^N v_p^* / N. \quad (73)$$

If no relaxation occurs for a particle p , $v_p^* = v_p$ applies. Using this approach, energy conservation is guaranteed and momentum conservation is ensured due to

$$\sum_{p=1}^N (v_p^* - u^*) = 0 \quad (74)$$

as described in Pfeiffer².

IV. SIMULATION RESULTS

The described multi-species ESBGK implementation including molecules with internal degrees of freedom is verified with simulation test cases of a supersonic Couette flow as well as a hypersonic flow around a 70° blunted cone. The different approaches for the calculation of the transport coefficients, Wilke's mixing rules (denoted by Wilke) and the collision integrals (denoted by CollInt), are compared using the VHS model.

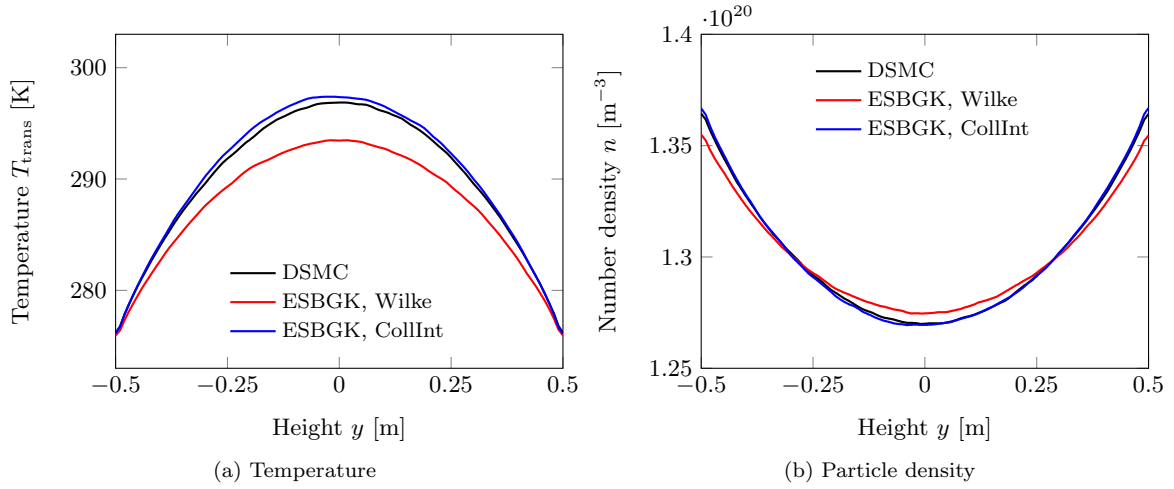
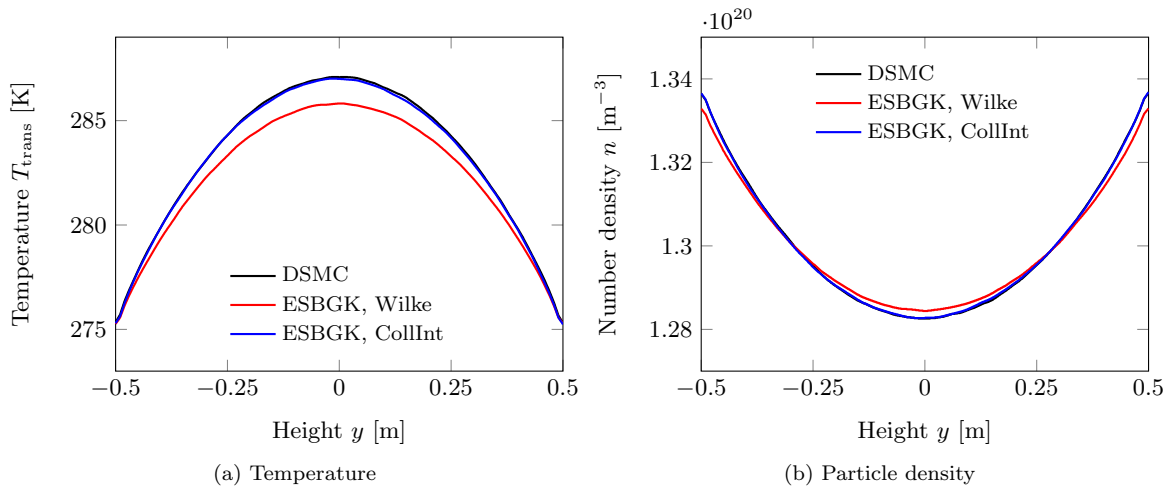
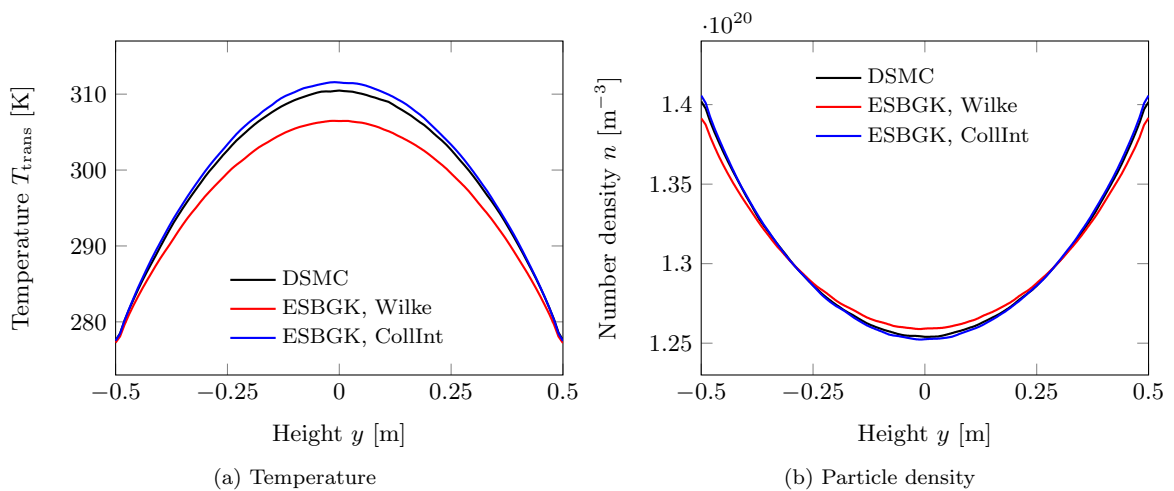
A. Supersonic Couette flow

The first test case is a three-dimensional simulation of a supersonic Couette flow. A mesh with 100 cells in y direction and a single cell in x and z directions is used. For the second test case of N₂-N with $Kn_{\text{VHS}} \approx 0.121$ and $Kn_{\text{VHS}} \approx 1.21$ as well as for test cases four and five, the mesh is refined and thus contains 400 cells in y direction. The time steps and particle weighting factors are chosen so that the mean free path and the collision frequency are resolved. The boundaries in y direction have a velocity of $v_{\text{wall},1} = 350 \text{ m s}^{-1}$ and $v_{\text{wall},2} = -350 \text{ m s}^{-1}$, respectively, assuming diffuse reflection and complete thermal accommodation at a constant wall temperature of $T_{\text{wall}} = 273 \text{ K}$. In x and z directions, all boundaries are periodic, leading to particles reappearing on a side after leaving the opposite side. Different gas mixtures are simulated, all initialized at $v_0 = 0 \text{ m s}^{-1}$ and $T_0 = 273 \text{ K}$.

First, a N₂-He mixture is simulated, which represents a challenging case due to the relatively large mass differences. Mixing ratios of 50%-50%, 20%-80% and 80%-20% with a initial particle density of $n_0 = 1.3 \cdot 10^{20} \text{ m}^{-3}$ are tested to estimate the influence of composition. In Figures 1, 2, and 3, the translational temperatures and particle densities are displayed for the different mixing ratios. In general, the ESBGK results using collision integrals are in excellent agreement with the DSMC results, while larger deviations up to 8.5 % are visible using Wilke's mixing rules due to the large mass ratio. The results slightly differ with the mixing ratio of N₂ and He. The 80 %-20 % N₂-He mixtures shows a maximum error of 3.6 % in the translational temperature between ESBGK with collision integrals and DSMC.

The second test mixture is a 50 %-50 % N₂-N mixture, initialized with the same particle density as for the first case, $n_0 = 1.3 \cdot 10^{20} \text{ m}^{-3}$, as well as lower densities by one and two orders of magnitude, respectively. This corresponds to Knudsen numbers of $Kn_{\text{VHS}} \approx 0.0121 - 1.21$, whereby the the implemented ESBGK method can be verified across different flow regimes. The results of these simulations for the translational temperatures and the particle densities are shown in Figures 4, 5, and 6. Again, the results of the ESBGK simulations using collision integrals are in very good agreement with the DSMC simulations. Due to the lower mass ratios, also Wilke's mixing rules achieve good agreement with the DSMC results. For higher Knudsen numbers, the errors for both ESBGK methods are increasing, which is in particular visible in Figure 6. Here, deviations of up to 32 % occur. The performance of the ESBGK method thus decreases for increasing Knudsen numbers.

As a third test case, a mixture with two molecular species (polyatomic and diatomic) is chosen: 50 %-50 % CO₂-N₂. Again, $n_0 = 1.3 \cdot 10^{20} \text{ m}^{-3}$ is the initial particle density. The results for the translational temperature and the particle density are depicted in Figure 7. All simulation methods show very good agreement with errors below 3.8 %.

FIG. 1. Comparison of the stationary solution for a supersonic Couette flow for a 50 %-50 % N_2 -He mixture.FIG. 2. Comparison of the stationary solution for a supersonic Couette flow for a 20 %-80 % N_2 -He mixture.FIG. 3. Comparison of the stationary solution for a supersonic Couette flow for a 80 %-20 % N_2 -He mixture.

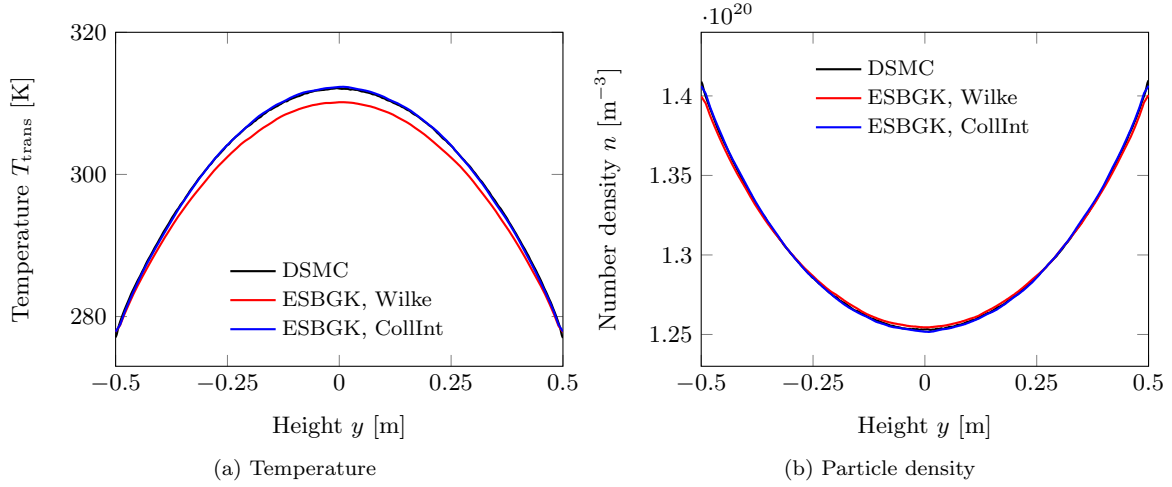


FIG. 4. Comparison of the stationary solution for a supersonic Couette flow for a 50%-50% N₂-N mixture with $Kn_{VHS} \approx 0.0121$.

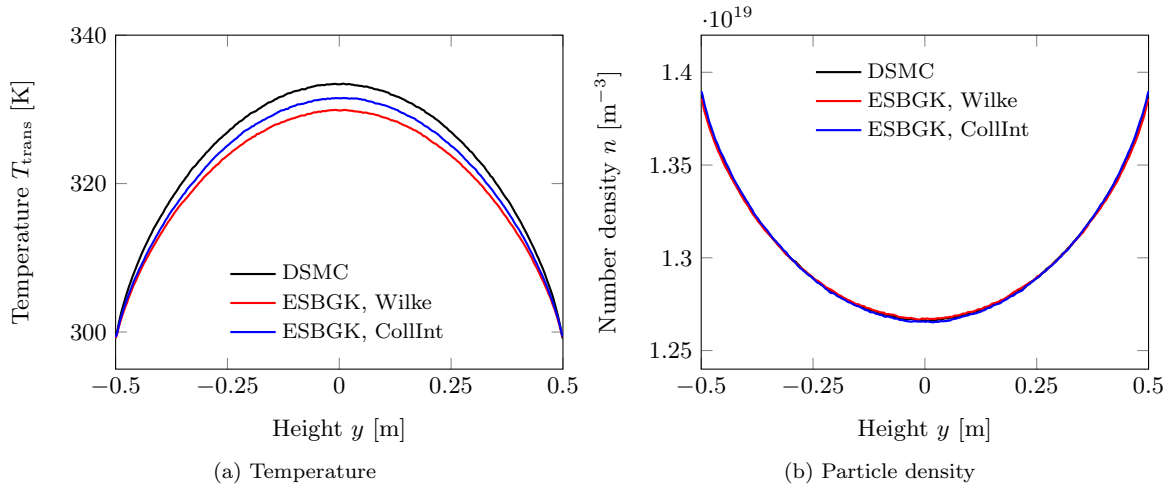


FIG. 5. Comparison of the stationary solution for a supersonic Couette flow for a 50%-50% N₂-N mixture with $Kn_{VHS} \approx 0.121$.

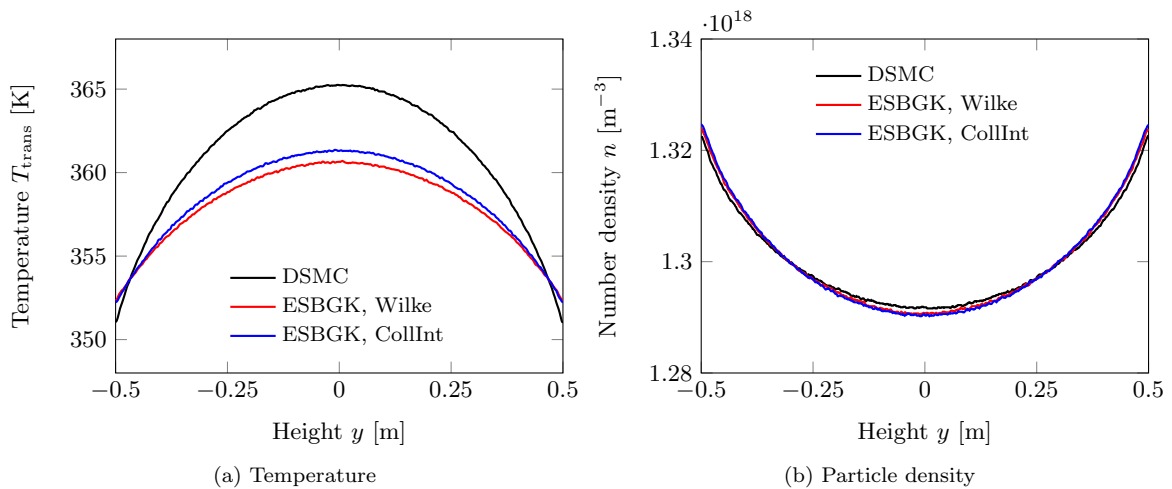


FIG. 6. Comparison of the stationary solution for a supersonic Couette flow for a 50%-50% N₂-N mixture with $Kn_{VHS} \approx 1.21$.

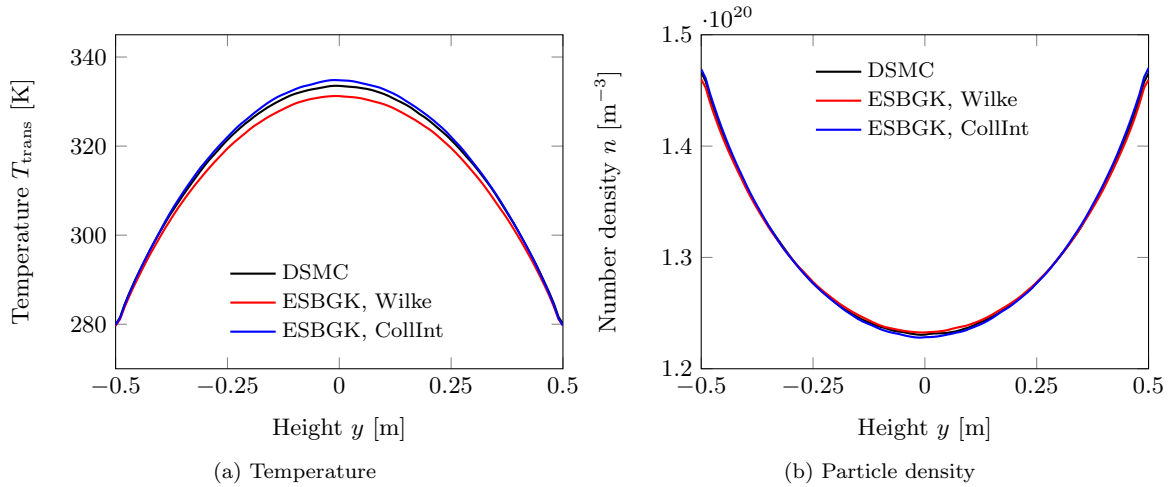


FIG. 7. Comparison of the stationary solution for a supersonic Couette flow for a 50 %-50 % CO₂-N₂ mixture.

With test cases four and five, two more realistic atmospheric gas mixtures with a larger number of constituents are simulated. From now on, only the DSMC and ESBGK solutions using collision integrals for the calculation of the transport coefficients are compared since the results using Wilke's mixing rules show larger errors, in particular when considering mixtures with large mass ratios.

Case four shows the results for a 78 %-21 %-1 % N₂-O₂-Ar mixture with $n_0 = 1.0 \cdot 10^{20} \text{ m}^{-3}$. In Figure 8, the results for the translational temperature and the particle density are compared. There is excellent agreement with deviations below 1.0 %.

For test case five, a N-O-N₂-O₂-NO mixture is chosen with each species contributing 20 % of the total gas with initial $n_0 = 1.25 \cdot 10^{20} \text{ m}^{-3}$. The ESBGK results show very good agreement with the DSMC results, both illustrated in Figure 9, with maximum deviations of 2.6 %.

B. 70 degree blunted cone

To test the behavior of the ESBGK mixture model in particular in the presence of strong gradients such as across shock waves, simulations of a hypersonic flow around a 70° blunted cone are done. The geometry of this model is illustrated in Figure 10. The simulations are performed two-dimensional axisymmetrical. At the surface of the cone diffuse reflection and complete thermal accommodation at a constant wall temperature of $T_{\text{wall}} = 300 \text{ K}$ is assumed. The inflow conditions are listed in Table I. A 50 %-25 %-25 % N₂-O₂-NO gas mixture is chosen for Cases 1-3, while a 50 %-50 % CO₂-N₂ mixture is used for Case 4. The mesh contains 5064 cells for Cases 1 and 4 with $1.06 \cdot 10^6$ total simulation particles and 16320 cells for Cases 2 and 3. For Case 2, $3.13 \cdot 10^6$ particles are in the simulation, while for Case 3, there

	Case 1	Case 2	Case 3	Case 4
Gas	N ₂ -O ₂ -NO	N ₂ -O ₂ -NO	N ₂ -O ₂ -NO	CO ₂ -N ₂
T_∞ / K	13.3	13.3	13.3	13.3
$u_\infty / \text{m s}^{-1}$	1502.57	1502.57	1502.57	1502.57
M_∞	20.7	20.7	20.7	23.2
n_∞ / m^{-3}	$3.7 \cdot 10^{20}$	$1.48 \cdot 10^{21}$	$5.92 \cdot 10^{21}$	$3.7 \cdot 10^{20}$
$Kn_{\text{VHS},\infty}$	0.147	0.0366	0.0092	0.108

TABLE I. Inflow conditions of hypersonic flow around a 70° blunted cone.

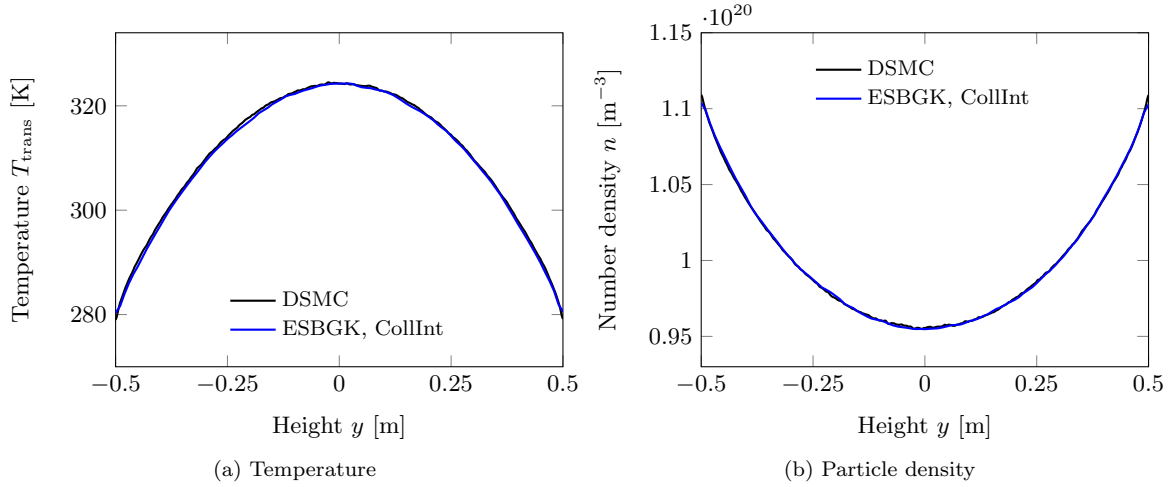
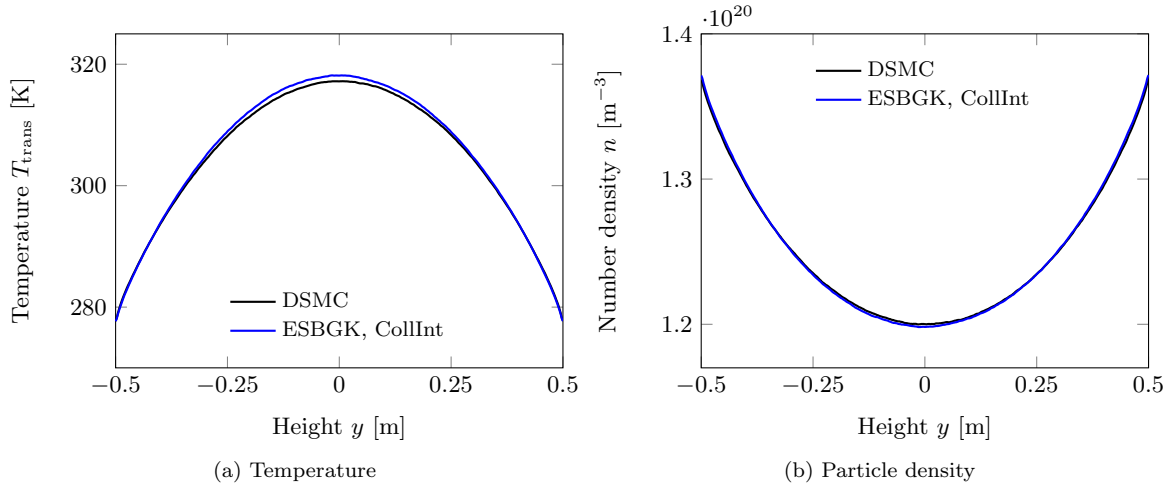
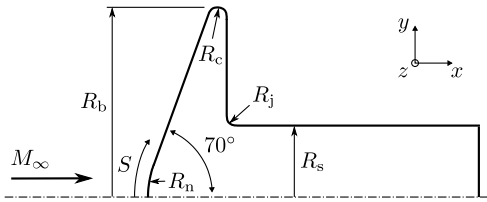
are $7.38 \cdot 10^6$ ESBGK simulation particles and $1.45 \cdot 10^7$ DSMC simulation particles, respectively. For the DSMC method, a time step of $1 \cdot 10^{-8} \text{ s}$ is used for Cases 1, 2 and 4, and a smaller time step is chosen for Case 3 with $2 \cdot 10^{-9} \text{ s}$, while for the ESBGK method, the time step is $2.5 \cdot 10^{-8} \text{ s}$. The results using Wilke's mixing rules and collision integrals are almost identical for all simulations, which is why the former are not shown separately.

1. Case 1

For the first test case, a particle density in the free-stream of $n_\infty = 3.7 \cdot 10^{20} \text{ m}^{-3}$ is assumed, corresponding to $Kn_{\text{VHS},\infty} = 0.147$, to show the abilities of the ESBGK model for non-equilibrium flows.

The simulation results of the mean flow variables of the mixture are shown in Figure 11. Overall good agreement is visible between the results of both methods.

In Figure 13, the mean translational, rotational and vibrational temperatures of the gas mixture are compared for the DSMC and ESBGK simulations. The ESBGK model predicts a earlier onset of the translational temperature increase compared to DSMC, which results in a wider shock region, also visible in Figure 12, where

FIG. 8. Comparison of the stationary solution for a supersonic Couette flow for a $\text{N}_2\text{-O}_2\text{-Ar}$ mixture.FIG. 9. Comparison of the stationary solution for a supersonic Couette flow for a $\text{N-O-N}_2\text{-O}_2\text{-NO}$ mixture.FIG. 10. Geometry of the 70° blunted cone. $R_b = 25.0$ mm, $R_c = 1.25$ mm, $R_j = 2.08$ mm, $R_n = 12.5$ mm, $R_s = 6.25$ mm. S denotes the arc length along the surface.

the translational temperature in the flow field is shown in comparison. The agreement in the post-shock region is excellent. Figure 13 also shows the vibrational temperatures of each species at $y = 20$ mm. Even in the non-equilibrium region in the wake of the 70° cone, the agreement between the results of the ESBGK and DSMC

methods is very good.

The heat flux on the cone surface is compared in Figure 14. For both the flow-facing cone surface as well as the rear cone part, excellent agreement between both methods is shown.

Different time steps and particle weighting factors are tested to find limits of the ESBGK method, where the simulation results are still in overall good agreement with the DSMC solution. Considering the computational costs, a comparison of the CPU time is done, where the ESBGK simulation is faster by a factor of ten compared to the DSMC simulation. For this, a time step of an order of magnitude larger than for the corresponding DSMC simulation could be chosen to still achieve a stable solution, and to resolve the relaxation time. The deviations in the results compared to DSMC are little increasing with a larger time steps, and with larger particle weighting factors in general, but the particle method is still stable.

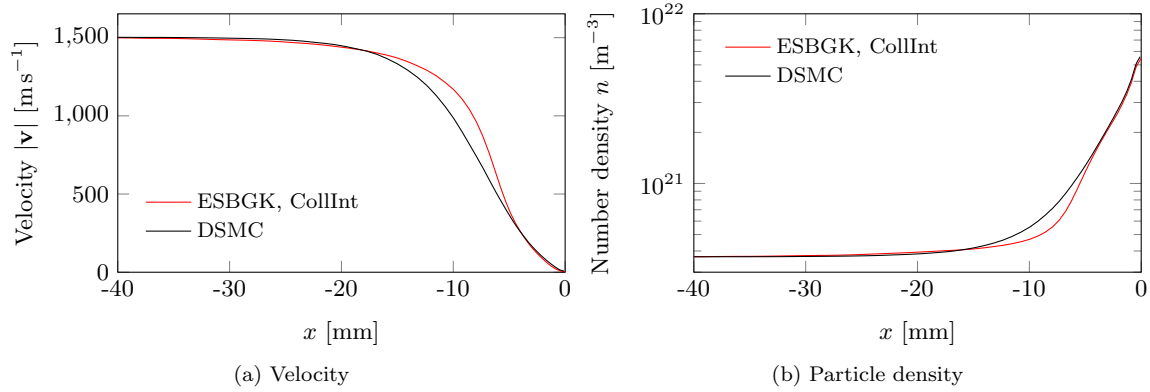


FIG. 11. 70° blunted cone, Case 1: Mixture mean values of velocity in x direction and number density along stagnation stream line using DSMC and ESBGK.

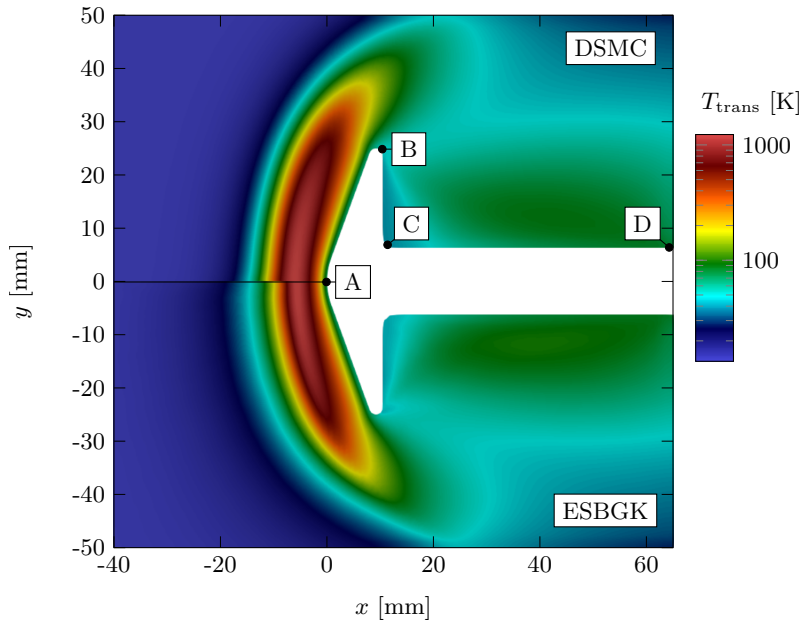


FIG. 12. 70° blunted cone, Case 1: Comparison of the mixture mean value of the translational temperature in the flow field using DSMC and ESBGK. Characteristic points A-D on the cone surface are indicated.

2. Case 2

As a second test case, a particle density in the free-stream of $n_{\infty} = 1.48 \cdot 10^{21} \text{ m}^{-3}$ is assumed, corresponding to $Kn_{\text{VHS},\infty} = 0.0366$, and representing a transitional regime case. With this, also the computational costs of both the DSMC and ESBGK methods are compared.

The simulation results of the mean values of the velocity in x direction and the particle density of the mixture are shown in Figure 15 with overall good agreement between the results of both methods.

In Figure 16, the mean translational, rotational and vibrational temperatures of the gas mixture are compared for the DSMC and ESBGK simulations. Similar to Case 1, the ESBGK model predicts an earlier onset of the

translational temperature increase compared to DSMC, resulting in a wider shock region. Excellent agreement is visible in the post-shock region. Figure 16 shows the vibrational temperatures of each species at $y = 20 \text{ mm}$ additionally. Again, there is very good agreement between the results of the ESBGK and DSMC methods even in the non-equilibrium region in the wake of the 70° cone.

A comparison of the heat flux on the cone surface is shown in Figure 17. For both the flow-facing cone surface as well as the rear cone part, both the ESBGK and the DSMC simulation results are in excellent agreement.

Considering the computational costs, a comparison of the CPU time is done. The ESBGK model reduces the CPU time by a factor of maximum 40.5 for the consid-

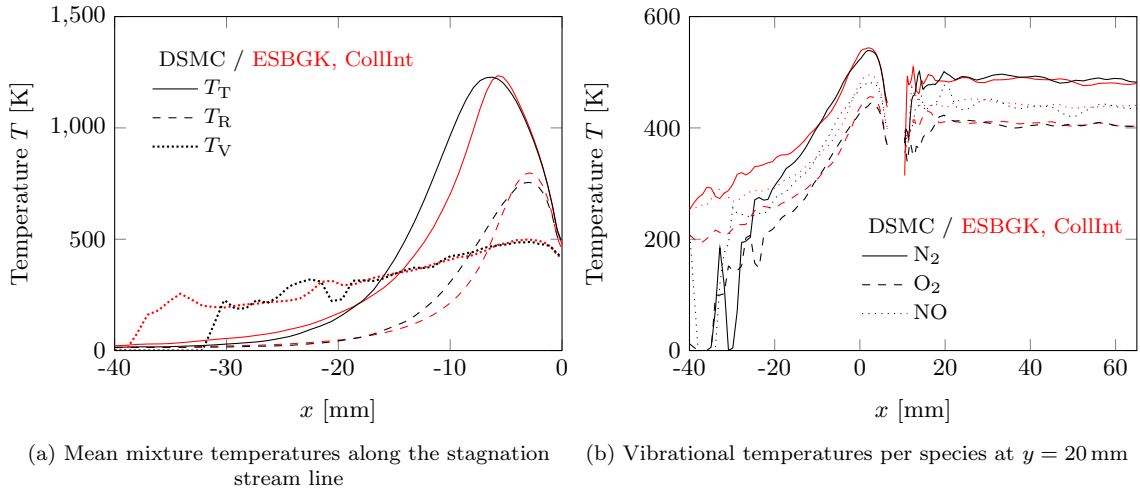


FIG. 13. 70° blunted cone, Case 1: Mixture mean values of the translation, rotational and vibrational temperatures along the stagnation stream line and species-specific values of the vibrational temperature at $y = 20$ mm using DSMC and ESBGK.

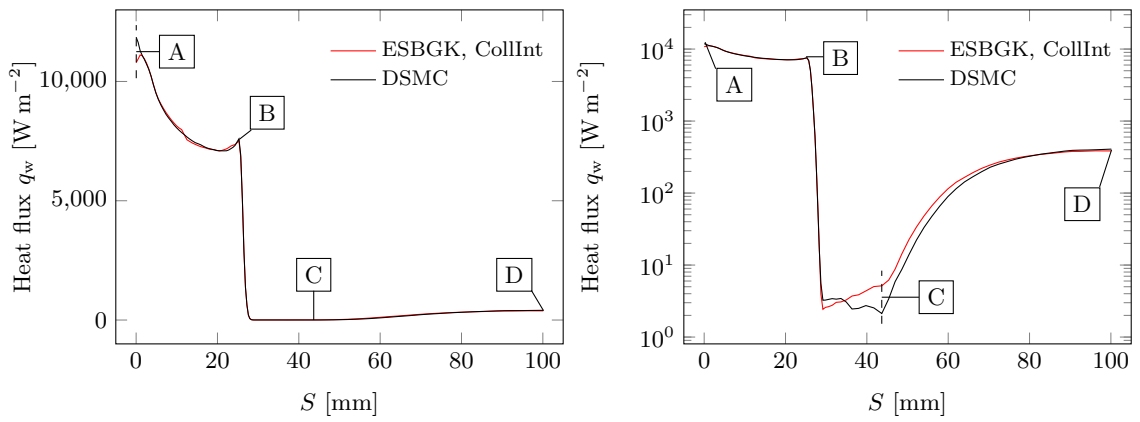


FIG. 14. 70° blunted cone, Case 1: Heatflux along the surface with characteristic points A-D indicated (see Figure 12).

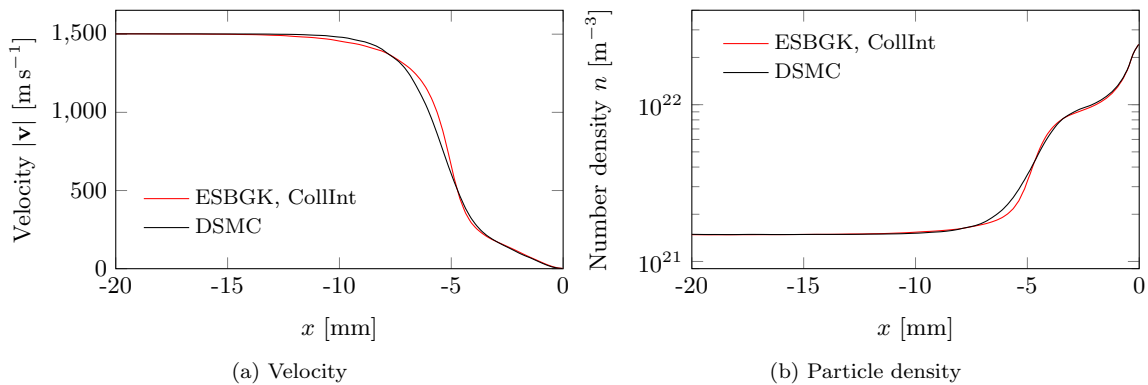


FIG. 15. 70° blunted cone, Case 2: Mixture mean values of velocity in x direction and number density along stagnation stream line using DSMC and ESBGK.

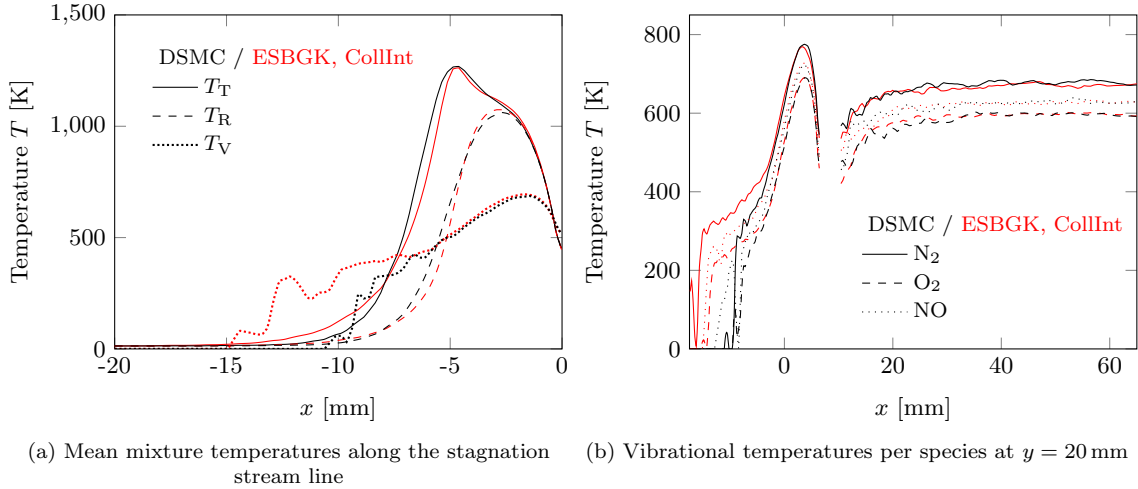


FIG. 16. 70° blunted cone, Case 2: Mixture mean values of the translation, rotational and vibrational temperatures along the stagnation stream line and species-specific values of the vibrational temperature at $y = 20$ mm using DSMC and ESBGK.

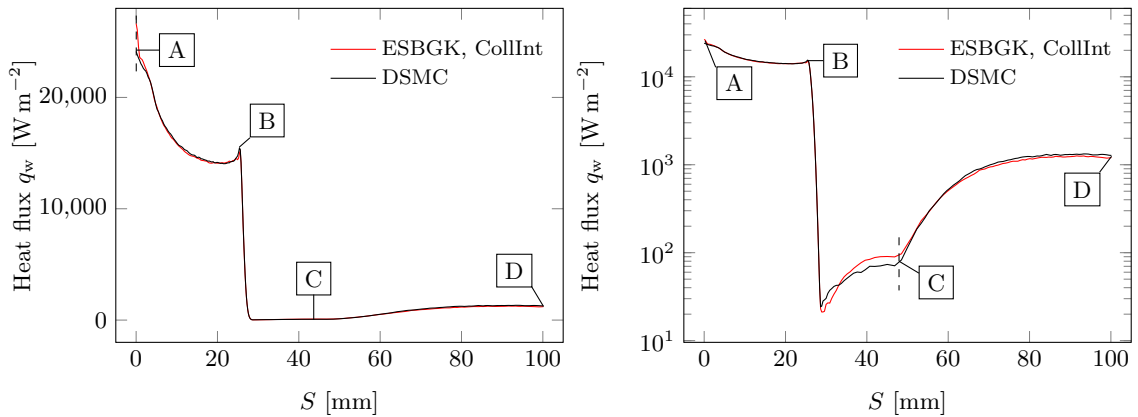


FIG. 17. 70° blunted cone, Case 2: Heatflux along the surface with characteristic points A-D indicated (see Figure 12).

ered test case without changing the simulation results. Here, the time step is chosen 40 times larger than for the corresponding DSMC simulation as a limit, and the relaxation time is still resolved.

3. Case 3

The third test case represents a continuum case with a particle density in the free-stream of $n_\infty = 5.92 \cdot 10^{21} \text{ m}^{-3}$, corresponding to $Kn_{VHS,\infty} = 0.0092$.

The the mean values of the velocity in x direction and the particle density of the mixture are compared in Figure 18 for the ESBGK and the DSMC models, both showing excellent agreement.

In Figure 19, the mean translational, rotational and vibrational temperatures of the gas mixture are shown. Compared to Cases 1 and 2, the earlier onset of the translational temperature increase of the ESBGK model

is very limited compared to DSMC. This is due to the higher density, leading to a narrower shock region in general. Again, excellent agreement is visible in the post-shock region. Furthermore, Figure 19 illustrates the vibrational temperatures of each species at $y = 20$ mm, showing good agreement with only little deviations in the non-equilibrium region in the wake of the 70° cone.

The simulation results for the heat flux on the cone surface is compared in Figure 20 for both of the models. There is good agreement of the results for the flow-facing cone surface as well as only little deviations for the rear cone part.

Same as for the other test cases, an additional comparison of the CPU time is done. The ESBGK simulation is initialised with a doubled weighting factor and a larger time step of factor 12.5 compared to the DSMC simulations. With this, both simulations are fully resolved, and the CPU time is reduced by a factor of 28.8.

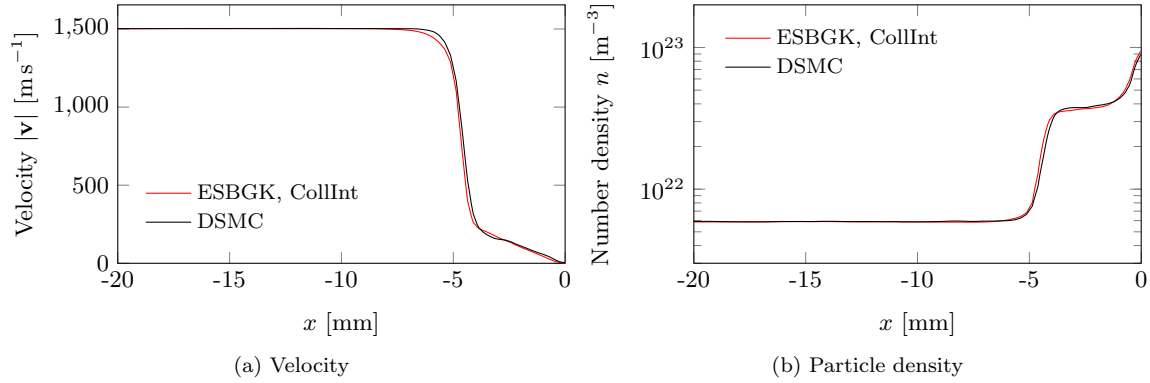


FIG. 18. 70° blunted cone, Case 3: Mixture mean values of velocity in x direction and number density along stagnation stream line using DSMC and ESBGK.

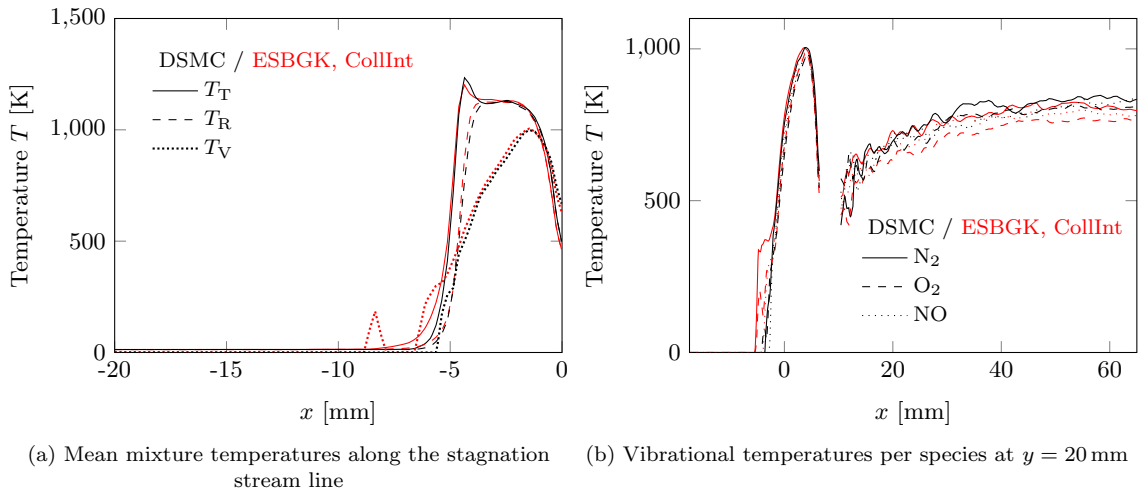


FIG. 19. 70° blunted cone, Case 3: Mixture mean values of the translation, rotational and vibrational temperatures along the stagnation stream line and species-specific values of the vibrational temperature at $y = 20$ mm using DSMC and ESBGK.

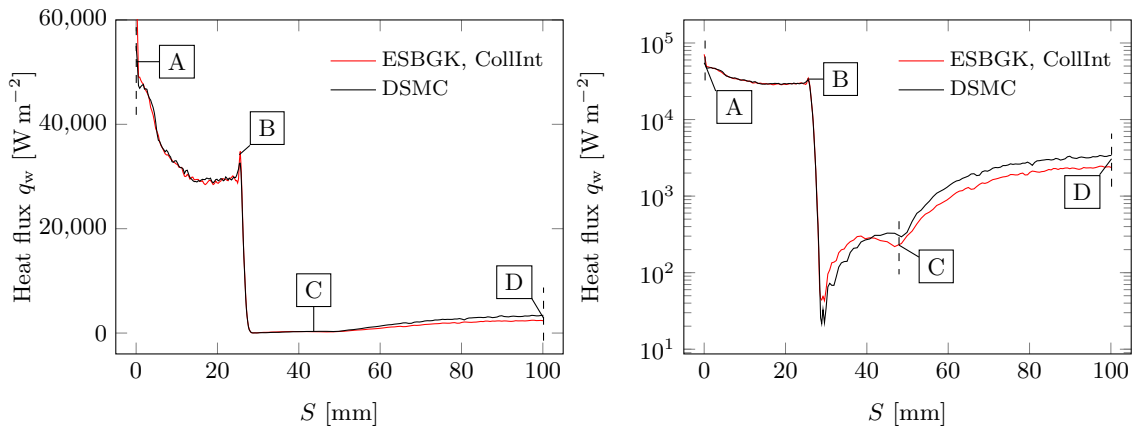


FIG. 20. 70° blunted cone, Case 3: Heatflux along the surface with characteristic points A-D indicated (see Figure 12).

4. Case 4

For Case 4, a 50 %-50 % $\text{CO}_2\text{-N}_2$ is chosen to evaluate the accuracy of the ESBGK model for a polyatomic-diatomic mixture with a higher number of degrees of internal freedom in particular in vibration. A particle density in the free-stream of $n_\infty = 3.7 \cdot 10^{20} \text{ m}^{-3}$ is chosen similarly to Case 1, which corresponds to $Kn_{\text{VHS},\infty} = 0.108$ for this mixture.

In Figure 21, the simulation results of the mean values of the velocity in x direction and the particle density of the mixture are compared for the DSMC and ESBGK models. Same as for the 50 %-25 %-25 % $\text{N}_2\text{-O}_2\text{-NO}$ gas mixture from Case 1, there is overall good agreement.

The mean translational, rotational and vibrational temperatures of the gas mixture are illustrated in Figure 22. Again, a wider shock region is visible for the ESBGK results due to an earlier onset of the translational temperature increase compared to DSMC, while there is very good agreement in the post-shock region. Also, the vibrational temperatures of each species at $y = 20 \text{ mm}$ are shown. While there is excellent agreement between the results of the ESBGK and DSMC methods in the non-equilibrium region in the wake of the 70° cone for N_2 , a small deviation can be seen for CO_2 .

The comparison of the heat flux on the cone surface in Figure 23 shows very good agreement.

Considering the CPU time, a reduction by factor 11.5 is possible with the ESBGK method. For that, the time step of the latter is chosen an order of magnitude larger than for the corresponding DSMC simulation as a limit, with which still a stable solution is achieved, and the relaxation time is resolved.

V. CONCLUSION

An ellipsoidal statistical BGK mixture method is proposed and implemented in the open-source particle code PICLas based on the model of Mathiaud, Mieussens, and Pfeiffer¹, Pfeiffer² and the model of Brull^{3,4}. With this, multi-species gas flows are simulated, while allowing for the treatment of internal energies of di- and polyatomic molecules. The aim is to use this particle-based continuum method for a coupling with the DSMC method to solve multi-scale problems. As test cases for verification, different supersonic Couette flows and flows around a 70° blunted cone are used. Hereby, also two methods for the determination of the transport coefficients of a gas mixture, Wilke's mixing rules and collision integrals, are compared. In general, overall good agreement between the ESBGK and DSMC methods is achieved for different type of mixtures and Knudsen numbers. Minor deviations occur concerning the onset of the temperature increase in the shock region in front of the 70° blunted cone. Also, the results using Wilke's mixing rules show larger errors compared to the DSMC results than using collision integrals to calculate the transport coefficients,

in particular for mixtures with large mass ratios. A considerable reduction of the computational duration is possible with the ESBGK method compared to DSMC.

In future work, the implementation of chemical reactions into the model is envisioned. Furthermore, an extension of the already implemented atomic Shakhov model to polyatomic gas mixtures will be done.

ACKNOWLEDGMENTS

This project has received funding from the European Research Council (ERC) under the European Union's Horizon 2020 research and innovation programme (grant agreement No. 899981 MEDUSA).

DATA AVAILABILITY

The data that support the findings of this study are available from the corresponding author upon reasonable request.

- ¹J. Mathiaud, L. Mieussens, and M. Pfeiffer, "An ES-BGK model for diatomic gases with correct relaxation rates for internal energies," *Eur. J. Mech. B/Fluids* **96**, 65–77 (2022).
- ²M. Pfeiffer, "Extending the particle ellipsoidal statistical Bhatnagar-Gross-Krook method to diatomic molecules including quantized vibrational energies," *Phys. Fluids* **30**, 116103 (2018).
- ³S. Brull, "An ellipsoidal statistical model for gas mixtures," *Commun. Math. Sci.* **13**, 1–13 (2014).
- ⁴S. Brull, "An ellipsoidal statistical model for a monoatomic and a polyatomic gas mixture," *Commun. Math. Sci.* **19**, 2177–2194 (2021).
- ⁵G. A. Bird, *Molecular Gas Dynamics and the Direct Simulation of Gas Flows* (Oxford University Press, New York, 1994).
- ⁶J. Zhang, B. John, M. Pfeiffer, F. Fei, and D. Wen, "Particle-based hybrid and multiscale methods for nonequilibrium gas flows," *Adv. Aerodyn.* **1**, 1–15 (2019).
- ⁷J. M. Burt and I. D. Boyd, "A low diffusion particle method for simulating compressible inviscid flows," *J. Comput. Phys.* **227**, 4653–4670 (2008).
- ⁸M. Pfeiffer, A. Mirza, and P. Nizenkov, "Evaluation of particle-based continuum methods for a coupling with the direct simulation Monte Carlo method based on a nozzle expansion," *Phys. Fluids* **31**, 073601 (2019).
- ⁹T. Schwartzenruber and I. Boyd, "A hybrid particle-continuum method applied to shock waves," *J. Comput. Phys.* **215**, 402–416 (2006).
- ¹⁰M. H. Gorji and P. Jenny, "An efficient particle Fokker-Planck algorithm for rarefied gas flows," *J. Comput. Phys.* **262**, 325–343 (2014).
- ¹¹M. Pfeiffer and M. H. Gorji, "Adaptive particle-cell algorithm for Fokker-Planck based rarefied gas flow simulations," *Comput. Phys. Commun.* **213**, 1–8 (2017).
- ¹²P. L. Bhatnagar, E. P. Gross, and M. Krook, "A Model for Collision Processes in Gases. I. Small Amplitude Processes in Charged and Neutral One-Component Systems," *Phys. Rev.* **94**, 511–525 (1954).
- ¹³M. A. Gallis and J. R. Torczynski, "Investigation of the ellipsoidal-statistical Bhatnagar-Gross-Krook kinetic model applied to gas-phase transport of heat and tangential momentum between parallel walls," *Phys. Fluids* **23**, 030601 (2011).
- ¹⁴H. L. Holway Jr., "New Statistical Models for Kinetic Theory: Methods of Construction," *Phys. Fluids* **9**, 1658–1673 (1966).

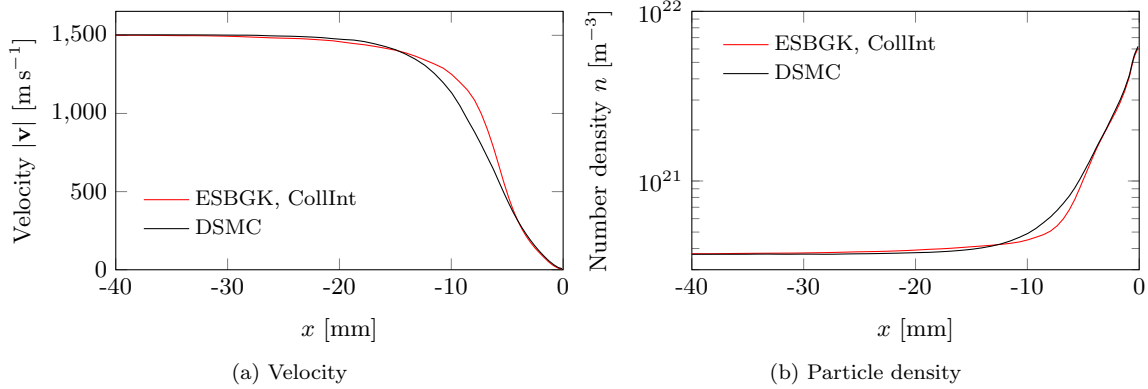


FIG. 21. 70° blunted cone, Case 4: Mixture mean values of velocity in x direction and number density along stagnation stream line using DSMC and ESBGK.

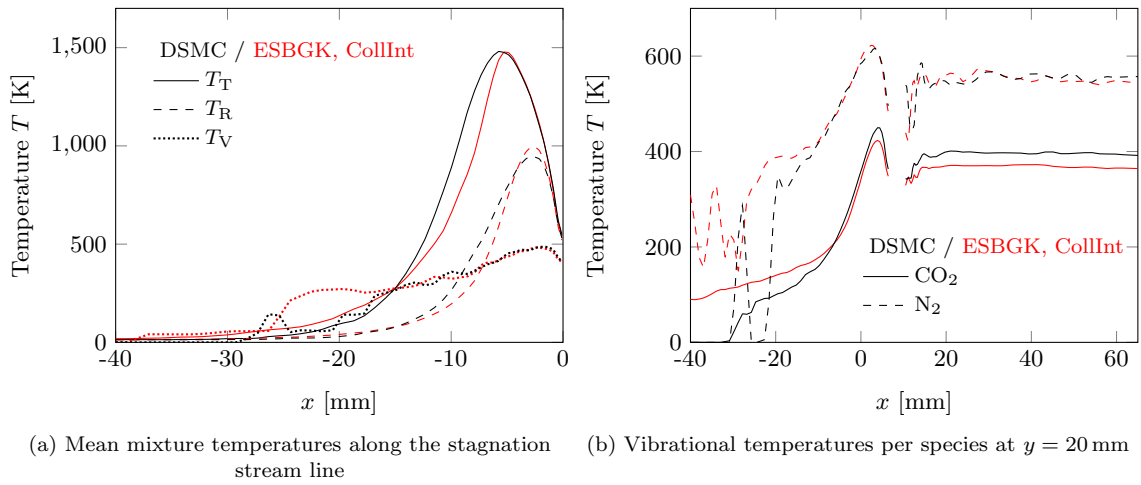


FIG. 22. 70° blunted cone, Case 4: Mixture mean values of the translation, rotational and vibrational temperatures along the stagnation stream line and species-specific values of the vibrational temperature at $y = 20$ mm using DSMC and ESBGK.

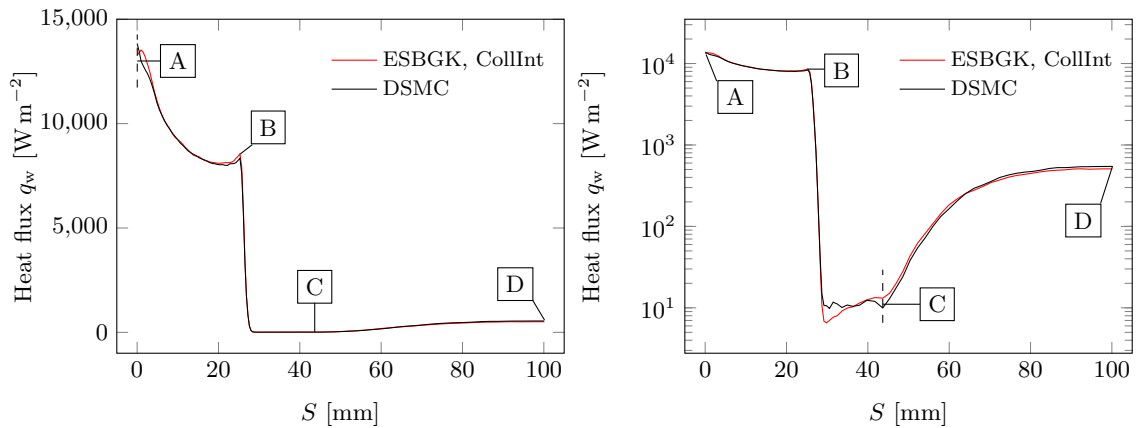


FIG. 23. 70° blunted cone, Case 4: Heatflux along the surface with characteristic points A-D indicated (see Figure 12).

- ¹⁵E. M. Shakhov, “Generalization of the Krook Kinetic Relaxation Equation,” *Fluid Dyn.* **33**, 95–96 (1968).
- ¹⁶M. Pfeiffer, “Particle-based fluid dynamics: Comparison of different Bhatnagar-Gross-Krook models and the direct simulation Monte Carlo method for hypersonic flows,” *Phys. Fluids* **30**, 106106 (2018).
- ¹⁷M. Pirner, “A Review on BGK Models for Gas Mixtures of Mono and Polyatomic Molecules,” *Fluids* **6**, 393 (2021).
- ¹⁸Y. Dauvois, J. Mathiaud, and L. Mieussens, “An ES-BGK model for polyatomic gases in rotational and vibrational nonequilibrium,” *Eur. J. of Mech. B/Fluids* **88**, 1–16 (2021).
- ¹⁹M. Pfeiffer, P. Nizenkov, A. Mirza, and S. Fasoulas, “Direct simulation Monte Carlo modeling of relaxation processes in polyatomic gases,” *Phys. Fluids* **28**, 027103 (2016).
- ²⁰G. Herzberg and B. L. Crawford Jr, “Infrared and Raman spectra of polyatomic molecules,” *J. Phys. Chem.* **50**, 288–288 (1946).
- ²¹C. R. Wilke, “A viscosity equation for gas mixtures,” *J. Chem. Phys.* **18**, 517–519 (1950).
- ²²J. O. Hirschfelder, C. F. Curtiss, and R. B. Bird, *The Molecular Theory of Gases and Liquids* (Wiley-Interscience, 1964).
- ²³S. Chapman and T. G. Cowling, *The Mathematical Theory of Non-uniform Gases* (Cambridge University Press, 1970).
- ²⁴K. Swaminathan-Gopalan and K. A. Stephani, “Recommended direct simulation Monte Carlo collision model parameters for modeling ionized air transport processes,” *Phys. Fluids* **28** (2016).
- ²⁵M. Pfeiffer, “An optimized collision-averaged variable soft sphere parameter set for air, carbon, and corresponding ionized species,” *Phys. Fluids* **34**, 117110 (2022).
- ²⁶A. Y. Hong and M. A. Gallis, “Optimized collision-specific parameters for binary mixtures of nitrogen, oxygen, argon, and helium,” *Phys. Fluids* **35** (2023).
- ²⁷J. B. Scoggins, V. Leroy, G. Bellas-Chatzigeorgis, B. Dias, and T. E. Magin, “Mutation++: MUlticomponent Thermodynamic And Transport properties for IONized gases in C++,” *SoftwareX* **12** (2020).
- ²⁸R. J. Kee, G. Dixon-Lewis, J. Warnatz, M. E. Coltrin, and J. A. Miller, *A Fortran computer code package for the evaluation of gas-phase multicomponent transport properties* (Sandia National Laboratories Report SAND86-8246, United States, 1986).
- ²⁹A. Ern and V. Giovangigli, *Eglib: A general-purpose fortran library for multicomponent transport property evaluation* (CERMICS Internal Report, 2004).
- ³⁰J. M. Burt and I. D. Boyd, “Evaluation of a Particle Method for the Ellipsoidal Statistical Bhatnagar-Gross-Krook Equation,” 44th AIAA Aerospace Sciences Meeting and Exhibit (2006).
- ³¹A. Eucken, “Über das Wärmeleitvermögen, die Spezifische Wärme und die innere Reibung der Gase,” *Phys. Z* **14** (1913).
- ³²J. O. Hirschfelder, “Heat conductivity in polyatomic or electronically excited gases. II,” *J. Chem. Phys.* **26**, 282–285 (1957).
- ³³K. A. Stephani, D. B. Goldstein, and P. L. Varghese, “Consistent treatment of transport properties for five-species air direct simulation Monte Carlo/Navier-Stokes applications,” *Phys. Fluids* **24**, 077101 (2012).
- ³⁴S. Fasoulas, C.-D. Munz, M. Pfeiffer, J. Beyer, T. Binder, S. Coplestone, A. Mirza, P. Nizenkov, P. Ortwein, and W. Reschke, “Combining particle-in-cell and direct simulation Monte Carlo for the simulation of reactive plasma flows,” *Phys. Fluids* **31**, 072006 (2019).
- ³⁵M. Pfeiffer, A. Mirza, and P. Nizenkov, “Multi-species modeling in the particle-based ellipsoidal statistical Bhatnagar-Gross-Krook method for monatomic gas species,” *Phys. Fluids* **33**, 036106 (2021).
- ³⁶M. Pfeiffer, A. Mirza, and P. Nizenkov, “Extension of Particle-based BGK Models to Polyatomic Species in Hypersonic Flow around a Flat-faced Cylinder,” *AIP Conference Proceedings* **2132**, 100001 (2019).
- ³⁷C. Chu, “Kinetic-theoretic description of the formation of a shock wave,” *Phys. Fluids* **8**, 12–22 (1965).
- ³⁸M. Pfeiffer, F. Garmirian, and M. H. Gorji, “Exponential Bhatnagar-Gross-Krook integrator for multiscale particle-based kinetic simulations,” *Phys. Rev. E* **106**, 025303 (2022).
- ³⁹M. A. Gallis and J. R. Torczynski, “The Application of the BGK Model in Particle Simulations,” 34th Thermophysics Conference, American Institute of Aeronautics and Astronautics, Denver, Colorado, USA (2000).